Journal of Statistical Physics, Vol. 52, Nos. 1/2, 1988

Mean Field Kinetic Theory of a Classical Electron Gas in a Periodic Potential. III. The High-Temperature Limit in Two Dimensions

Angel Alastuey,[1] Jean Clérouin,[2] and Jean-Pierre Hansen[2,3]

Received February 19, 1988

The Vlasov-like mean field kinetic equation for a classical electron plasma in the periodic field of an ionic lattice is solved in the high-temperature limit in two dimensions. The predictions for the one-electron density, the static structure factor, and the long-wavelength charge fluctuation spectrum are compared to the results of extensive molecular dynamics simulations. The predicted shift and damping of the plasma oscillation mode are in reasonable agreement with the simulation data at intermediate couplings ($\Gamma = e^2/k_B T \simeq 1$), but the agreement deteriorates as the temperature or the density is lowered, because mean field theory does not lead to the expected Kosterlitz–Thouless transition to the dielectric phase where electrons are localized.

KEY WORDS: Classical electron gas; periodic potential; Vlasov approximation; plasmon mode; damping; shift.

1. INTRODUCTION

The classical two-component plasma made up of oppositely charged ions and electrons is particularly interesting in two dimensions (2D), where it undergoes a Kosterlitz–Thouless (KT) transition between a high-temperature plasma phase and a low-temperature dielectric phase.[1,2] A fixed-ion version of the 2D two-component plasma in which the positive ions occupy the sites of a triangular lattice exhibits interesting single-particle

[1] Laboratoire de Physique Théorique et Hautes Energies (Laboratoire associé au Centre National de la Recherche Scientifique), Université de Paris-Sud, 91405 Orsay, France.
[2] Commissariat à l'Energie Atomique, Centre d'Etudes de Limeil-Valenton, 94190 Villeneuve-St-Georges, France.
[3] Ecole Normale Supérieure de Lyon, 69364 Lyon, France.

0022-4715/88/0700-0395$06.00/0

and collective dynamical behavior in the vicinity of the transition due to the gradual "recombination" of ions and electrons, which has been extensively studied by molecular dynamics (MD) simulations.[3,4] The fixed-ion model, which will be the subject of this paper, is isomorphous to a one-component (OCP) of classical electrons in a periodic field. In view of a theoretical analysis of the dielectric response and collective dynamics of the model, a mean field kinetic equation has recently been formulated.[5] General consequences of the mean field theory have been derived in paper I of this series for arbitrary D,[6] while explicit solutions for the 1D case were obtained in paper II.[7] The main conclusions of the mean field analysis are that the model remains a conductor (i.e., stays in the plasma phase) at all temperatures, independent of dimensionality, and that plasma oscillations are damped by the coupling of the mobile electrons to the ion lattice even in the long-wavelength ($k \to 0$) limit; the damping increases rapidly and the frequency of the plasmon resonance is shifted below the plasma frequency as the temperature is lowered. While the first of these conclusions contradicts the existence of a dielectric phase in 1D[8] and in 2D,[2] the predictions concerning the dynamics of charge oscillations in 1D[7] agree qualitatively with available MD simulation results in 2D.[3]

In the present paper we extend the 1D analysis of mean field theory contained in paper II to the 2D fixed-ion model in the high-temperature limit and compare the predictions to extensive MD simulations carried out under identical physical conditions. This study is motivated by the need to gain a microscopic understanding of the influence of ionization equilibria in dense plasmas on the collective dynamics of the electrons; such equilibria can be modeled in purely classical terms in 2D due to the binding nature of the logarithmic Coulomb interaction.

2. THE MODEL

We consider a two-component plasma made up of ρ ions and as many electrons per unit area carrying charges $+e$ and $-e$, respectively. The Coulomb potential between equal charges is, in 2D,

$$\Phi_c(r) = -e^2 \ln(r/L_s) \tag{2.1}$$

where L_s is an irrelevant scale length. The ion–electron potential must be regularized at short distances in order to avoid the collapse of opposite charges at low temperatures[9]; as in ref. 4, we adopt the following potential:

$$\begin{aligned} \Phi_{ie}(r) &= \Phi_{SR}(r), \qquad r < \sigma \\ &= -\Phi_C(r), \qquad r > \sigma \end{aligned} \tag{2.2}$$

where the short-range part (SR) is chosen to be parabolic:

$$\Phi_{\mathrm{SR}}(r) = e^2[\ln(\sigma/L_s) - \tfrac{1}{2}] + \tfrac{1}{2}e^2(r^2/\sigma^2) \tag{2.3}$$

This form ensures continuity of the potential and of the force at $r = \sigma$. By adding two compensating uniform background charge densities $\pm e\rho$, the total potential energy of the system is easily cast in the form

$$V_N(\mathbf{r}_1, \ldots, \mathbf{r}_N) = V_0(\mathbf{r}_1, \ldots, \mathbf{r}_N) + U_0 + \sum_{i=1}^{N} V_L(\mathbf{r}_i) \tag{2.4}$$

where the $\mathbf{r}_i$ are electron positions, V_0 is the potential energy of the 2D OCP of mobile electrons in a uniform positive background, U_0 is the Madelung energy of the ion lattice, and $V_L(\mathbf{r})$ is the periodic potential of the ion lattice (L) seen by the electrons:

$$V_L(\mathbf{r}) = \int d\mathbf{r}'\, \Phi_{\mathrm{C}}(|\mathbf{r} - \mathbf{r}'|) \left[\rho - \sum_j \delta(\mathbf{r}' - \mathbf{R}_j) \right] + \Phi_{\mathrm{ie}}(r) + \Phi_{\mathrm{C}}(r) \tag{2.5}$$

where $\mathbf{r}$ belongs to the Wigner–Seitz unit cell WS centered on the site $\mathbf{R}_0 = 0$, and the sum is over all ionic lattice sites; in writing (2.5) we have assumed $\sigma < b$, where $b = (\pi/2\sqrt{3})^{1/2}\, a$ is half the distance between nearest neighbor sites, and $a = (\pi\rho)^{-1/2}$ is the "ion-disk" radius.

The Fourier components of the lattice potential $V_L(\mathbf{r})$ are

$$\begin{aligned} \hat{V}_L(\mathbf{G}) &= \rho \int_{\mathrm{WS}} d\mathbf{r}\, V_L(\mathbf{r}) \exp(i\mathbf{G} \cdot \mathbf{r}) \\ &= -4\pi e^2 \rho (J_1(G\sigma)/G^3\sigma), \qquad G \neq 0 \\ \hat{V}_L(0) &= \pi e^2 \rho \sigma^2/4 \end{aligned} \tag{2.6}$$

where $\mathbf{G}$ are reciprocal lattice vectors and J_1 is the cylindrical Bessel function of order 1.

A thermodynamic state of the model is characterized by the number density ρ, or equivalently by the dimensionless ratio σ/a, and by the Coulomb coupling constant $\Gamma = e^2/k_{\mathrm{B}}T$. For the two-component system, a theoretical analysis of the static dielectric constant shows that the KT critical coupling is 4 in the zero-density limit. For the present model, such an analysis is not yet available. However, MD simulations[3,4] indicate that the KT critical coupling goes to 2 when σ/a goes to zero; in particular, the conductivity decreases by several orders of magnitude in the vicinity of this critical coupling. Since the MD simulations are carried out on finite systems, the above prediction regarding the KT transition must be con-

sidered cautiously. In fact, there are several scenarios that are consistent with the MD observations. For instance, the conductivity might be very small between $\Gamma = 2$ and $\Gamma = 4$ (because there are very few free charges), but might strictly vanish only at $\Gamma = 4$. The present study is restricted to the high-temperature plasma phase ($\Gamma \leqslant 1$), where mean field theory is expected to apply.

3. PREDICTIONS OF MEAN FIELD THEORY AT HIGH TEMPERATURES

The results of paper I for the static properties of the model are easily adapted to the 2D case. In the high-temperature limit, the one-particle density $[\rho(\mathbf{r})]$ solution of Eq. (I.3.10) reduces to

$$\rho(\mathbf{r}) = \rho\{1 - \beta[V_L(\mathbf{r}) - \hat{V}_L(0)] + O(\beta^2)\} \tag{3.1a}$$

where

$$\begin{aligned} V_L(\mathbf{r}) - \hat{V}_L(0) &= \sum_{\mathbf{G}\neq 0} \hat{V}_L(\mathbf{G}) \exp(i\mathbf{G}\cdot\mathbf{r}) \\ &= \frac{-4\pi\rho e^2}{\sigma} \sum_{\mathbf{G}\neq 0} \frac{J_1(G\sigma)}{G^3} \exp(i\mathbf{G}\cdot\mathbf{r}) \end{aligned} \tag{3.1b}$$

It is tempting to exponentiate the result (3.1a) and to renormalize it so that the integral of the exponentiated expression over WS remains equal to 1, i.e., to set

$$\rho(\mathbf{r}) = \text{const} \times \exp\{-\beta[V_L(\mathbf{r}) - \hat{V}_L(0)]\} \tag{3.2}$$

The expressions (3.1a) and (3.2) will be compared to molecular dynamics results in Section 4.

The main result of the mean field analysis in paper I is that the electron density response function can be cast in the suggestive generic form

$$\chi(\mathbf{k}, \omega) = -\beta\rho \frac{k^2 T(\mathbf{k}, \omega)}{k^2 + \chi_D^2 T(\mathbf{k}, \omega)} \tag{3.3}$$

where χ_D^2 is the square of the Debye screening wavenumber of the homogeneous OCP ($\chi_D^2 = 2\pi\rho e^2/k_B T = 2\Gamma/a^2$ in 2D) and the function $T(\mathbf{k}, \omega)$ may be formally expressed in terms of the electron trajectories in the self-consistent mean field [cf. Eq. (I.4.25)]. In the much simpler uniform background case, $T(\mathbf{k}, \omega)$ is related to the response function of a noninteracting gas with free-particle trajectories.

The static structure factor $S(\mathbf{k})$ is proportional to the $\omega = 0$ limit of the response function (3.3),

$$S(\mathbf{k}) = \frac{1}{N}\langle \rho_{\mathbf{k}} \rho_{-\mathbf{k}} \rangle = \frac{-1}{\beta\rho}\chi_{(\mathbf{k},\omega=0)} = \frac{k^2 T(\mathbf{k})}{k^2 + \chi_D^2 T(\mathbf{k})} \tag{3.4}$$

where the explicit form of $T(\mathbf{k}) = T(\mathbf{k}, \omega = 0)$ is given in Eq. (I.5.4). If the one-particle densities appearing in that expression are replaced by their high-temperature form (3.1), $T(\mathbf{k})$ reduces to

$$\begin{aligned} T(\mathbf{k}) &= 1 - \beta^3 \sum_{G \neq 0} \hat{V}_L(\mathbf{G})\, \hat{V}_L(-\mathbf{G}) \frac{2\pi\rho e^2}{|\mathbf{G} - \mathbf{k}|^2} + O(\beta^4) \\ &= 1 - 32\Gamma^3 \sum_{G \neq 0} \frac{[J_1(\sigma G)]^2}{\sigma^2 a^6 G^6\, |\mathbf{G} - \mathbf{k}|^2} + O(\Gamma^4) \end{aligned} \tag{3.5}$$

When $\Gamma \to 0$, the standard Debye–Hückel formula, valid for the uniform background case, is recovered for $S(\mathbf{k})$. The leading high-temperature correction to that limit is obtained by including the Γ^3 term in Eq. (3.5). Note that Eq. (3.5) is valid as long as $\mathbf{k}$ does not coincide with a reciprocal lattice vector ($\mathbf{k} \neq \mathbf{G}$). However, $T(\mathbf{G})$ is a well-defined quantity, as shown in Appendix B of paper II.

For small k, $S(\mathbf{k})$ may be expanded as

$$S(\mathbf{k}) = \frac{k^2}{\chi_D^2}\left[1 - \frac{k^2}{k_s^2} + O(k^4)\right] \tag{3.6}$$

where the screening wavenumber k_s is related to the isothermal compressibility.[10,3] Combination of the mean field Eqs. (3.4) and (3.5) leads to the high-temperature result

$$\begin{aligned} k_s^2 &= \chi_D^2 T(0) \\ &= \chi_D^2 \left\{1 - 32\Gamma^3 \sum_{G \neq 0} \frac{[J_1(\sigma G)]^2}{\sigma^2 a^6 G^8} + O(\Gamma^4)\right\} \end{aligned} \tag{3.7}$$

It was shown in paper I that $T(0) > 0$ for all Γ, independent of dimensionality, so that mean field theory implies $S(k) \sim k^2/\chi_D^2$ and hence that the system is a conductor at all temperatures; in the high-temperature limit k_s reduces to χ_D, while the leading high-temperature correction leads to a *reduction* of the screening wavenumber, i.e., a reduction of the screening capacity of the inhomogeneous plasma compared to its homogeneous counterpart.

It is amusing to note that, while the exact mean field $T(0)$ is strictly positive, its high-temperature expression in Eq. (3.7) vanishes when

$$\Gamma^{-3} = 32 \sum_{G \neq 0} \frac{[J_1(G\sigma)]^2}{(G\sigma)^8} \left(\frac{\sigma}{a}\right)^6 \tag{3.8}$$

In the low-density limit $\sigma/a \to 0$, this leads to the estimate $\Gamma \simeq 3.91$ of the coupling at the plasma–dielectric transition, which is closer to $\Gamma = 4$ than to $\Gamma = 2$. Of course, this does not constitute a conclusive argument in favor of the former value for the KT critical coupling. Moreover, Eq. (3.8) predicts that the critical Γ increases with σ/a, in agreement with recent MD results.[4]

Turning now our attention to the dynamical response, we examine the predictions of mean field theory for the dynamical structure factor

$$S(\mathbf{k}, \omega) = -\frac{1}{\pi\rho\beta\omega} \chi''(\mathbf{k}, \omega) = \frac{1}{2\pi} \int_{-\infty}^{+\infty} dt\, e^{i\omega t} F(\mathbf{k}, t) \tag{3.9}$$

where, according to the fluctuation-dissipation theorem, χ'' is the imaginary part of the density response function (3.3), while $F(\mathbf{k}, t)$ denotes the density–density correlation function (or intermediate scattering function)

$$F(\mathbf{k}, t) = \frac{1}{N} \langle \rho_{\mathbf{k}}(t)\, \rho_{-\mathbf{k}}(0) \rangle, \qquad \rho_{\mathbf{k}}(t) = \sum_{i=1}^{N} \exp[i\mathbf{k} \cdot \mathbf{r}_i(t)] \tag{3.10}$$

More specifically, we have evaluated the mean field expression for the long-wavelength limit of the normalized spectrum

$$s(\omega) = \lim_{k \to 0} \frac{S(\mathbf{k}, \omega)}{S(\mathbf{k})} \tag{3.11}$$

In paper I it was shown that $s(\omega)$ can be cast in the generic form

$$s(\omega) = \frac{I(\omega)}{\pi\omega\{[1 + R(\omega)]^2 + I^2(\omega)\}} \tag{3.12a}$$

$$R(\omega) = \mathrm{Re}\{W_1(\omega) + W_2(\omega)\} \tag{3.12b}$$

$$I(\omega) = \mathrm{Im}\{W_1(\omega) + W_2(\omega)\} \tag{3.12c}$$

Explicit expressions for the functions $W_1(\omega)$ and $W_2(\omega)$ in terms of the electron trajectories in the self-consistent periodic potential are given in Eqs. (I.6.7), (I.6.8). Detailed results for the 1D case are presented in paper II. The situation in 1D is relatively simple, because of the simplicity

of the confined and unconfined trajectories of the electrons in the periodic self-consistent field. The main result of paper II is that $s(\omega)$ exhibits a damped plasmon resonance, which is shifted below the plasma frequency ω_p. The shift and the damping are proportional to $\Gamma^{3/2}$ (where $\Gamma = \beta e^2 a$ in 1D). The collective plasmon mode vanishes in the limit $\Gamma \to \infty$.

The situation is considerably more complicated in 2D, because of the great complexity of the electron trajectories. However, the trajectories that yield the dominant contributions to $W_1(\omega)$ and $W_2(\omega)$ in the high-temperature limit are the high-energy trajectories in the periodic lattice potential $V_L(\mathbf{r})$ defined by (3.1b), which is the limit form of the full self-consistent potential $V(\mathbf{r})$. To study these contributions, it is convenient to introduce the sequence of auxiliary potentials

$$V_{L,s}(\mathbf{r}) = \hat{V}_L(0) + 2 \sum_{j=1}^{s} \sum_{p=1}^{\infty} \hat{V}_L(p\mathbf{G}_j) \cos(p\mathbf{G}_j \cdot \mathbf{r}) \tag{3.13}$$

where the $\mathbf{G}_j$ are the s smallest reciprocal lattice vectors of the form

$$\mathbf{G}_j = (m_j \mathbf{A} + n_j \mathbf{B})$$

with $\mathbf{A}$ and $\mathbf{B}$ the basis vectors of the reciprocal lattice, and (m_j, n_j) pairs of mutually prime integers; the corresponding $\mathbf{G}_j$ define a set of orientations that are all different. The high-temperature forms of $W_1(\omega)$ and $W_2(\omega)$ will be calculated for $V_{L,s}(\mathbf{r})$ and, the limit $s \to \infty$, which leads back to the full lattice potential $V_L(\mathbf{r})$, will be taken at the end.

Let $r_{cl}(t; \mathbf{r}, \mathbf{v})$ and $v_{cl}(t; \mathbf{r}, \mathbf{v})$ denote the position and velocity of a particle at time t calculated from the equations of motion in the force field of the potential $V_{L,s}(\mathbf{r})$, with initial conditions $r_{cl}(0; \mathbf{r}, \mathbf{v}) = \mathbf{r}$ and $v_{cl}(0; \mathbf{r}, \mathbf{v}) = \mathbf{v}$. Then, as long as the initial velocity is not orthogonal to any of the $\mathbf{G}_j$, the velocity increment at time t is given by a standard perturbation expansion around the free particle trajectory $\mathbf{r}_0(t; \mathbf{r}, \mathbf{v}) = \mathbf{r} + \mathbf{v}t$, namely

$$\mathbf{u}(t) = \mathbf{v}_{cl}(t; \mathbf{r}, \mathbf{v}) - \mathbf{v} = \frac{2}{mv} \sum_{j=1}^{s} \frac{\mathbf{G}_j}{(\mathbf{G}_j \cdot \hat{\mathbf{v}})} \sum_{p=1}^{\infty} \hat{V}_L(p\mathbf{G}_j) \times [\cos(p\mathbf{G}_j \cdot \mathbf{r}) - \cos(p\mathbf{G}_j \cdot \mathbf{r} + p\mathbf{G}_j \cdot \mathbf{v}t)] + O\left(\frac{1}{v^2}\right) \tag{3.14}$$

valid when $v \to \infty$ for fixed $\hat{\mathbf{v}} = \mathbf{v}/v$ and $\hat{\mathbf{v}} \cdot \mathbf{G}_j \neq 0$ for all j. However, as soon as $\hat{\mathbf{v}}$ is "almost" orthogonal to one of the $\mathbf{G}_j$, Eq. (3.14) becomes inapplicable. In this case, the motion projected along $\mathbf{G}_j$ cannot be studied

through a perturbative treatment of the potential $2\sum_{p=1}^{\infty}\hat{V}_L(p\mathbf{G}_j)\cos(p\mathbf{G}_j\cdot\mathbf{r})$ because the latter is no longer small compared to the kinetic energy $m(\mathbf{v}\cdot\hat{\mathbf{G}}_j)^2/2$. In the Appendix we analyze this motion in the limit where the component of the initial velocity orthogonal to $\mathbf{G}_j$ goes to infinity. It is these trajectories that yield the dominant contributions to $W_1(\omega)$ and $W_2(\omega)$, which are $O(1/v)$ and are explicitly given in the Appendix. The resulting expressions for $R(\omega)$ and $I(\omega)$ read

$$R(\omega)=-\frac{\omega_p^2}{\omega^2}+\Gamma^{3/2}r(\omega)+o(\Gamma^{3/2}) \tag{3.15a}$$

$$I(\omega)=\Gamma^{3/2}i(\omega)+o(\Gamma^{3/2}) \tag{3.15b}$$

where

$$\begin{aligned} r(\omega)&=\sum_{j=1}^{\infty} r_j(\omega)\\ &=\frac{1}{\pi^{1/2}a^3\omega_p}\,\mathrm{Re}\sum_{j=1}^{\infty}\rho\int_{\mathrm{WS}}d\mathbf{r}\int_{-\infty}^{+\infty}dv_j\lim_{\eta\to 0^+}\left(\int_0^{\infty}dt\,e^{i\omega t-\eta t}\right.\\ &\quad\left.\times\left\{[x_j(t)-v_jt-x_j][v_j(t)-v_j]+\frac{1}{2i\omega}(1-i\omega t)[v_j(t)-v_j]^2\right\}\right) \end{aligned} \tag{3.16}$$

and $i(\omega)$ is equal to the imaginary part of the same expression. The integrals appearing in (3.16) are evaluated by the techniques developed for the 1D case in paper II. Details, as well as final expressions for the $r_j(\omega)$ and corresponding $i_j(\omega)$, are contained in the Appendix. Here $\omega_p=(2\pi\rho e^2/m)^{1/2}$ is the 2D plasma frequency.

As in 1D, the leading correction to the uniform background limit in Eqs. (3.15) is proportional to $\Gamma^{3/2}$. When $\Gamma\to 0$, the dynamical structure factor (3.12a) reduces to the usual uniform Vlasov limit, i.e., a pair of δ-functions centered on $\omega=\pm\omega_p$. The leading high-temperature correction leads both to a broadening and a shift of the position of the two conjugate plasmon peaks in $s(\omega)$ relative to ω_p. If restriction is made to the immediate vicinity of the peak at positive frequencies, $s(\omega)$ may be approximated by a Lorentzian centered on

$$\omega_m=\omega_p[1-\Gamma^{3/2}(r(\omega_p)/2)] \tag{3.17}$$

where $r(\omega_p)$ must be calculated numerically from the expressions listed in the Appendix. The resulting $r(\omega_p)$ is always positive, so that the plasmon mode is shifted *below* the plasma frequency ω_p by the coupling of the elec-

trons to the ion lattice. As the temperature is lowered, the shift increases as $\Gamma^{3/2}$. For ω close to ω_m, set $\omega = \omega_m + \Gamma^{3/2}\nu$; then

$$s(\omega_m + \Gamma^{3/2}\nu) \sim \frac{\omega_p i(\omega_p)}{\pi\Gamma^{3/2}[\omega_p^2 i^2(\omega_p) + 4\nu^2]} \tag{3.18}$$

which represents a Lorentzian of full-width at half-maximum

$$\Delta\omega = \Gamma^{3/2}\omega_p i(\omega_p) \tag{3.19}$$

while the height of the peak is

$$s(\omega_m) = \frac{1}{\pi\Gamma^{3/2}\omega_p i(\omega_p)} \tag{3.20}$$

Thus, the plasmon is seen to be damped even in the limit of infinite wavelength due to the "friction" of the electrons against the ion lattice (electron–ion collisions). This damping mechanism vanishes in the uniform background limit, but becomes increasingly important as the temperature is lowered, because electrons get "trapped" by individual ions; the term "recombinational damping" was coined in ref. 3 for this mechanism. Results (3.18)–(3.20) are of a form identical to that found at high temperatures for the 1D case,[7] the only differences being the numerical values of $r(\omega_p)$ and $i(\omega_p)$.

In view of the fact that the mean field calculation of this section incorporates only the leading correction to free-particle motion, it is important to ascertain the range of validity of its predictions by explicit comparison with the results of "exact" molecular dynamics simulations carried out on the same model.[4] This is the purpose of the next section.

4. COMPARISON WITH MOLECULAR DYNAMICS RESULTS

In order to test the predictions of mean field theory for the one-particle density $\rho(\mathbf{r})$, the static structure factor $S(\mathbf{k})$, and the long-wavelength charge fluctuation spectrum $s(\omega)$, we have extended our previous MD simulations of the model[4] to higher temperatures. The earlier simulations were more concerned with the Kosterlitz–Thouless "localization" transition, both for the present model, embodied in Eqs. (2.2)–(2.3), and for a hard-core version of the model[3] in which the ions strongly repel the electrons for $r < \sigma$. However in the corresponding range of coupling ($\Gamma > 2$) the high-temperature results of the mean field analysis are not expected to be applicable *a priori*, so that simulations at higher temperatures ($\Gamma \simeq 1$) are clearly required to allow a meaningful comparison. It must be realized,

however, that MD simulations tend to become inefficient at high temperatures, since the occurrence of increasingly "hard" collisions between particles forces the use of shorter and shorter time steps in the numerical solution of the finite-difference version of the equations of motion. Such a shortening of the time step is incompatible with long trajectories in phase space, which are needed to obtain good statistics, particularly for the collective charge fluctuation spectrum. We have compromised by exploring the range $2 > \Gamma > 1$, using the standard Verlet algorithm[11] and rectangular simulation cells containing $N = 120$ or 168 electrons (and as many ions) with periodic boundary conditions. Nearly square rectangular cells, rather than the more natural hexagonal cells used in the hard-core simulations,[3] were employed in the present work in order to simplify the Ewald summations of the Coulomb interactions over periodic images of all the charges. Several densities were explored, namely $\sigma/a = \sqrt{2}/8$, $\sqrt{2}/4$, $\sqrt{2}/2$, and 1. If $\omega_0 = (e^2/m\sigma^2)^{1/2}$ denotes the vibration frequency in the harmonic potential well (2.3) of the ion–electron potential, these densities correspond to ratios $\omega_0/\omega_p = 4$, 2, 1, and $\sqrt{2}/2$. Most runs extended over a total time interval of $1000\omega_p^{-1}$ after equilibration, which correspond typically to 10^5 time steps. A summary of the characteristics of the MD runs is given in Table I.

The angular-averaged one-particle density has been calculated inside the Wigner–Seitz disk of radius a. A comparison with the high-temperature prediction (3.1a) of mean field theory is made in Fig. 1. The exact $\rho(r)$ is significantly more localized than the linearized mean field expression (3.1a), especially at lower temperature or lower density. Note, however, that the exponentiated result (3.2) agrees much better with the MD data, even at $\Gamma = 2$. The observed differences are due to the effects of the linearization of the mean field solution and to the electron–electron correlations, which are not included in the mean field treatment.

Table I. Characteristics of Molecular Dynamics Runs[a]

σ/a	Γ	N_t	$\omega_p \Delta t$	$\omega_p t_m$
0.177	1.022	10^5	10^{-2}	10^3
	1.934	10^5	10^{-2}	10^3
0.354	0.982	10^5	10^{-2}	10^3
	1.943	10^5	10^{-2}	10^3
0.707	1.096	10^5	10^{-2}	10^3
1.0	1.001	10^5	10^{-2}	10^3

[a] N_t is the total number of time steps Δt; $t_m = N_t \Delta t$ is the total time interval covered by the run.

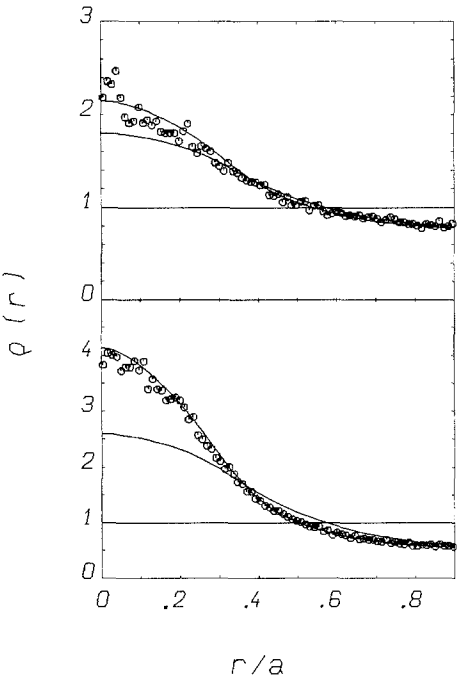

Fig. 1. One-electron density $\rho(r)$ versus r/a for $\sigma/a = 0.354$ and $\Gamma = 1$ (upper curves) and $\Gamma = 2$ (lower curves). The dots are the MD data, while the curves are the high temperature mean field result (3.1a) and the exponentiated form (3.2); the latter result falls right on the MD data.

Similarly, we have computed the angular-averaged static structure factor $S(k)$ for wavevectors compatible with the periodic boundary conditions. Standard fluctuation theory leads to the following long-wavelength form[3] of $S(k)$:

$$S(k) \underset{k \to 0}{\sim} \frac{k^2}{\chi_D^2(1 + k^2/k_s^2)} \tag{4.1}$$

where the screening wavenumber k_s is related to the isothermal compressibility χ_T by $k_s^2 = \chi_D^2(\chi_T/\chi_T^{(0)})$, $\chi_T^{(0)}$ being the compressibility of an ideal gas at the same temperature and density. In the mean field approximation, $\chi_T/\chi_T^{(0)} = T(0)$ according to Eq. (3.7). We have determined the screening wavenumber by fitting the MD data at small k to the limit (4.1). The resulting values are compared to the mean field predictions in Table II. The latter lie close to and slightly below the Debye wavenumber χ_D, whereas the "exact" ratio k_s/χ_D first increases above 1 as the temperature is lowered,

Table II. Screening Wavenumbers[a]

σ/a	Γ	$(k_s/\chi_D)_{m.f.}$	$(k_s/\chi_D)_{MD}$
0.177	1.022	0.992	1.092
	1.934	0.947	1.104
0.354	0.982	0.995	1.092
	1.943	0.964	1.19
	4.46	0.344	0.557
0.707	1.096	0.999	1.2
1.0	1.001	0.99998	1.32

[a] k_s/χ_D is the ratio of the screening wavenumber k_s over the Debye wavenumber $\chi_D = (2\pi\rho e^2/k_B T)^{1/2} = (2\Gamma)^{1/2}/a$.

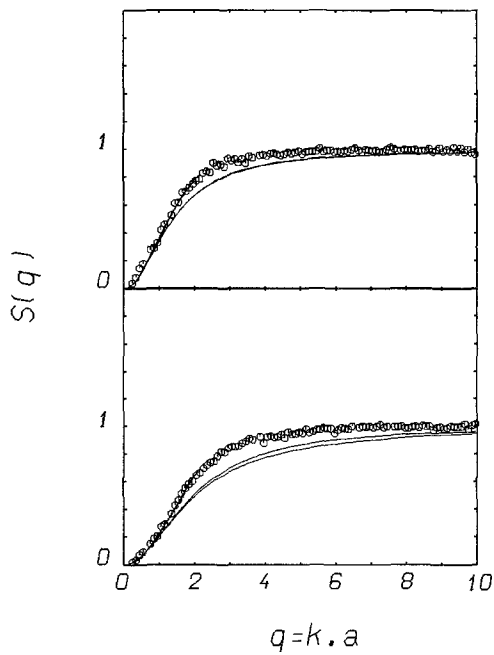

Fig. 2. Angular-averaged static structure factor $S(k)$ versus $q = ka$ for $\sigma/a = 0.354$ and $\Gamma = 1$ (upper curves) and $\Gamma = 2$ (lower curves). The dots are the MD data. For $\Gamma = 1$, the solid curve is the mean field result (3.4), which practically coincides with the homogeneous Debye–Hückel result [i.e., with $T(\mathbf{k}) = 1$]. For $\Gamma = 2$ the mean field result is represented by the lower curve; the homogeneous Debye–Hückel result falls between the latter result and the MD data.

before decreasing at still lower temperatures due to incipient localization; k_s is expected to vanish at the dielectric–plasma transition.[3] In the plasma phase electron–electron correlations lead to an increase of the screening power of the Coulomb gas compared to the mean field results, which only incorporate the ion–electron coupling. At $\Gamma \simeq 1$, the mean field structure factor deviates very little from the uniform background Debye–Hückel limit $S(k) = k^2/(k^2 + \chi_D^2)$, while the MD results lie above this limit for all k. The density appears to hardly affect $S(k)$ for a given Γ, whereas the difference between mean field and MD results is more pronounced at lower temperature, as shown in Fig. 2.

The quantity of main interest is the long-wavelength charge fluctuation spectrum $s(\omega)$, defined in (3.11). The MD simulations yield the intermediate scattering function (3.10) for wavevectors $\mathbf{k}$ compatible with the periodic boundary conditions, i.e., $\mathbf{k} = 2\pi(n_x/L_x, n_y/L_y)$, where L_x and L_y are the side lengths of the rectangular simulation cell and n_x, n_y are integers which cannot be simultaneously zero. Due to the near-degeneracy ($L_x \simeq L_y$) of our cells, averages may be taken over nearly equivalent $\mathbf{k}$ vectors. The $k \to 0$ limit, i.e., $s(\omega)$, can only be obtained indirectly, by calculating the normalized electric current autocorrelation function $J(t)$, which determines the frequency-dependent conductivity $\sigma(\omega) = \sigma'(\omega) + i\sigma''(\omega)$ and coincides with the memory function of the long-wavelength charge density autocorrelation function,[3] i.e.,

$$s(\omega) = \frac{2\sigma'(\omega)}{[\omega - 2\pi\sigma''(\omega)]^2 + [2\pi\sigma'(\omega)]^2} \tag{4.2}$$

By identification with (3.12a), we find that the mean field expressions for $\sigma'(\omega)$ and $\sigma''(\omega)$ are

$$2\pi\sigma'(\omega) = \omega I(\omega) \tag{4.3a}$$

$$2\pi\sigma''(\omega) = -\omega R(\omega) \tag{4.3b}$$

In particular, since it has been shown[6] that $R(\omega) = O(1/\omega^2)$ and $I(\omega) = O(1/\omega^2)$ for small ω, the static conductivity predicted by mean-field theory diverges, and correspondingly $\lim_{\omega \to 0} s(\omega) = 0$ due to the absence of dissipation originating in electron–electron collisions.

For each of the runs listed in Table I we have computed $J(t)$ and $F(\mathbf{k}, t)$ for several wavenumbers $\mathbf{k}$. Typical examples are shown in Figs. 3 and 4. The value of $J(t)$ is affected by considerable statistical noise, but is seen to decrease monotonically more and more slowly as σ/a increases. The spectra $s(\omega)$ and $S(k, \omega)/S(k)$ are obtained by numerical Fourier transformation. A partial check of the numerical accuracy of the results follows

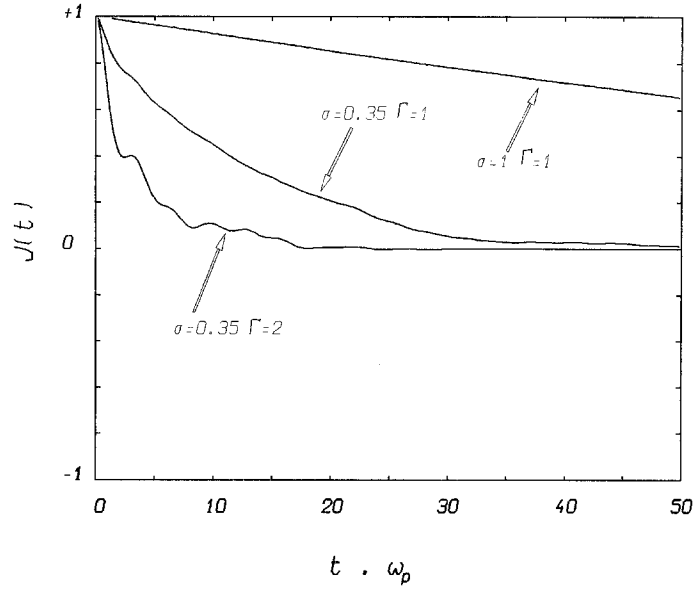

Fig. 3. Normalized electric current autocorrelation function $J(t)$ versus $\omega_p t$, as calculated by MD for $\sigma/a = 1$ and $\Gamma = 1$ (upper curve); and $\sigma/a = 0.35$, $\Gamma = 1$, and $\Gamma = 2$ (lower curve). Notice the appearance of small oscillations in the latter case, characteristic of incipient electron localization.[3]

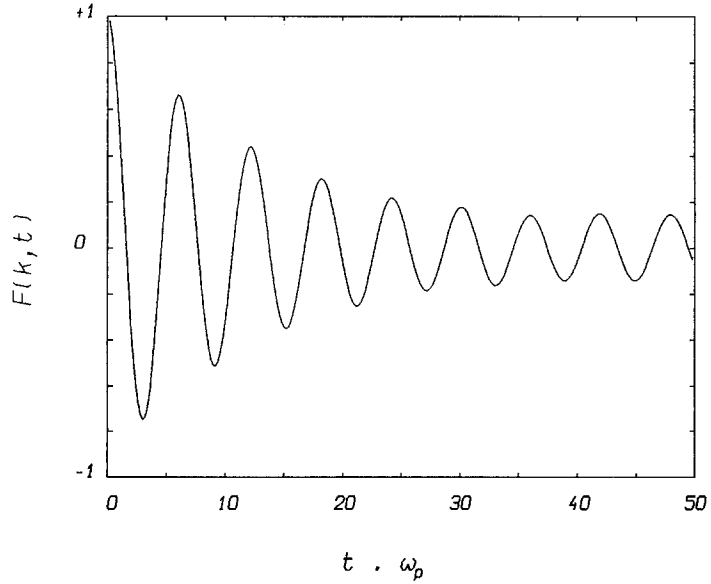

Fig. 4. MD-generated normalized density autocorrelation function $F(k, t)$ versus $\omega_p t$ for $\sigma/a = 0.354$, $\Gamma = 1$, and $q = ka = 0.275$.

from the usual frequency sum rules. The familiar second moment sum rule is

$$\overline{\omega^2} = \int_{-\infty}^{+\infty} \omega^2 \frac{S(\mathbf{k}, \omega)}{S(\mathbf{k})}\, d\omega = \frac{k_B T}{m} \frac{k^2}{S(\mathbf{k})} \xrightarrow[k \to 0]{} \omega_p^2 \tag{4.4}$$

while the fourth moment sum rule reads in the present case

$$\begin{aligned}\overline{\omega^4} &= \int_{-\infty}^{+\infty} \omega^4 \frac{S(\mathbf{k}, \omega)}{S(\mathbf{k})}\, d\omega \\ &= \frac{1}{S(\mathbf{k})} \left\{ \left(\frac{k_B T}{m} k^2 \right)^2 \right. \\ &\quad + \frac{k_B T}{m^2} \int_{WS} d\mathbf{r}\, \rho(\mathbf{r}) (\mathbf{k} \cdot \nabla)^2 V_L(\mathbf{r}) \\ &\quad \left. + \frac{k_B T}{m^2} \int g(\mathbf{r}) (\mathbf{k} \cdot \nabla)^2 \Phi_C(r) [1 - \exp(i\mathbf{k} \cdot \mathbf{r})]\, d\mathbf{r} \right\}\end{aligned} \tag{4.5}$$

where the periodic potential $V_L(\mathbf{r})$ of the ion lattice is given by Eq. (2.5), $\Phi_C(r)$ is the Coulomb potential (2.1), $\rho(\mathbf{r})$ is the one-particle density of the electrons, and $g(\mathbf{r})$ is the electron–electron pair distribution function. Up to the order k^2 included, $\overline{\omega^2}$ and $\overline{\omega^4}$ are isotropic functions of $\mathbf{k}$. Furthermore, these moments will be computed approximately, with a good accuracy, by replacing the various functions involved in (4.4), (4.5) by their angular-averaged counterparts. The corresponding expression for $\overline{\omega^4}$ is greatly simplified:

$$\begin{aligned}\frac{\overline{\omega^4}}{\omega_p^4} &\simeq 3 \frac{k^2}{\chi_D^2} + 1 + \pi \frac{a^2}{\sigma^2} \int_0^\sigma \Delta\rho(r) r\, dr + \int_0^\infty [g(r) - 1] J_2(kr) \frac{dr}{r} \\ &\underset{k \to 0}{=} 1 + \pi \frac{a^2}{\sigma^2} \int_0^\sigma \Delta\rho(r) r\, dr\end{aligned} \tag{4.6}$$

where $\Delta\rho(r) = \rho(r) - \rho$.

Results based on expressions (4.4) and (4.6) have been compared to the second and fourth frequency moments directly calculated from the computer-generated spectra; discrepancies do not exceed a few percent, thus giving us confidence in the MD data (with the limitations exposed in footnote 5).

In the discussion of the results, we first concentrate on the long-wavelength spectra $s(\omega)$, which may be compared directly to the mean field predictions of Section 3 and more specifically to the high-temperature

Table III. Mean Field Lorentzian Width Parameter $i(\omega_p)$

σ/a	0.177	0.354	0.707	0.952
$i(\omega_p)$	0.297	0.238	0.010	0.00062

Lorentzian form (3.18). The inputs needed are the values of $i(\omega_p)$ and $r(\omega_p)$, the expressions for which are given in the Appendix. The numerical evaluation of $i(\omega_p)$ is relatively simple, and results for the densities of interest are given in Table III. The calculation of $r(\omega_p)$ is more involved, but a simple sum-rule argument based on Eq. (4.4), with a Lorentzian suitability truncated at $\omega = 0$ [where the mean field $s(\omega)$ vanishes] and at $\omega = 2\omega_m$ [where $\omega^2 s(\omega)$ goes through a minimum] leads to the estimate $r(\omega_p) = i(\omega_p)/\pi$, which we have adopted for the comparison with the MD data.[4] Comparisons for $\Gamma \simeq 1$ and for two densities are made in Figs. 5 and 6. Both sets of results exhibit a negative shift of the plasmon resonance with respect to ω_p. The width of the spectrum (i.e., the damping of the electron

[4] We have checked that $r(\omega_p)$ behaves like $i(\omega_p)$ when $\sigma/a \to 0$. For finite values of σ/a, one should have $i(\omega_p)/\pi < r(\omega_p) < i(\omega_p)$. Note that, for σ/a sufficiently large, an accurate calculation of $r(\omega_p)$ is not essential for the comparison with the MD data, because $r(\omega_p)$ is then very small and the MD simulations do not allow us to distinguish between ω_m and ω_p.

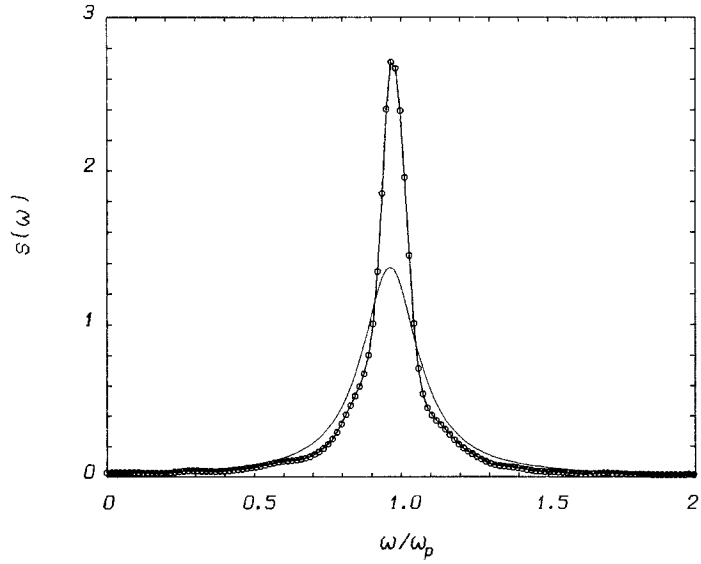

Fig. 5. Long-wavelength charge fluctuation spectrum $s(\omega)$ versus ω/ω_p for $\sigma/a = 0.354$, $\Gamma = 1$. (- -) MD data; (–) high-temperature mean field result (3.18).

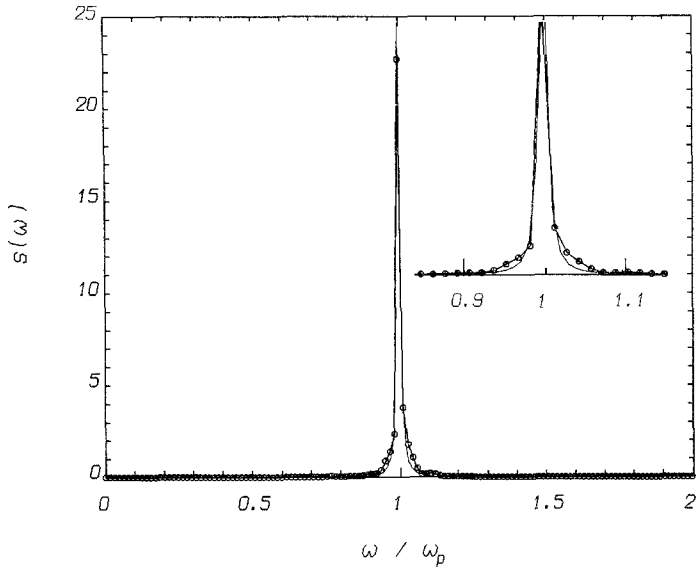

Fig. 6. Same as Fig. 5, but for $\sigma/a = 0.707$, $\Gamma = 1$; insert: same curves in the vicinity of the maximum.

plasma oscillations) appears to be overestimated by the high-temperature mean field approximation at the lower densities, but slightly underestimated in the limit $\sigma \to a$. The damping and the shift of the plasmon mode decrease with increasing density; the peaks are already very sharp at $\sigma/a = 0.71$. This dramatic reduction of the damping is a direct consequence of the observation made in ref. 4 that the periodic potential of the ions perturbs the electrons only weakly when $\sigma/a \to 1$, so that the electron plasma behaves practically as an OCP in a uniform background. In that limiting case, conservation of the total momentum of the electrons would imply the reduction of $s(\omega)$ to a pair of δ-functions centered on $\pm\omega_p$.[12] As expected, the difference between the mean field and "exact" results for $s(\omega)$ is much more pronounced at lower temperatures, as illustrated in Fig. 7. This is not a surprise, since the mean field results incorporate only the leading high-temperature contribution. However, mean field theory reproduces the main qualitative trends, in particular the increasing shift of the characteristic plasmon frequency ω_m below ω_p. This shift is similar to that observed within the hard-core model,[3] and may be interpreted in terms of a partial recombination (or electron localization), which reduces the number of "free" electrons participating in the collective plasma oscillations and hence the effective plasma frequency. The effect is opposite to that observed in dense electron–proton plasmas in 3D, where the

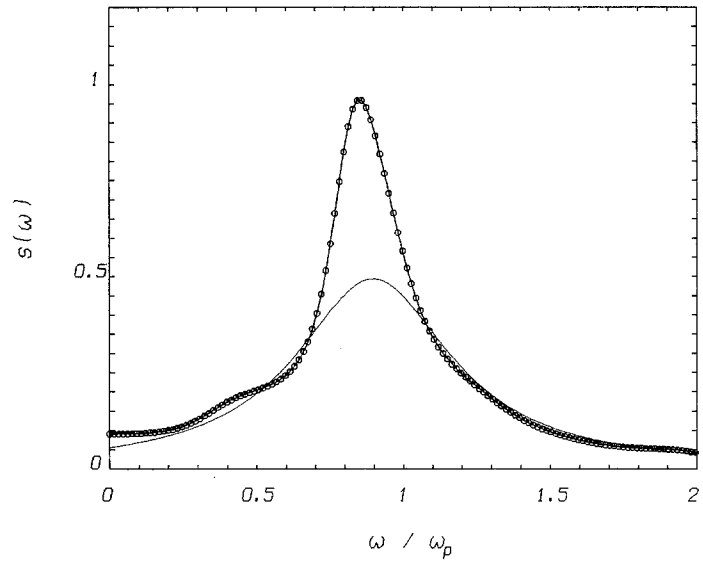

Fig. 7. Same as Fig. 5, but for $\sigma/a = 0.354$, $\Gamma = 2$; note that the Lorentzian approximation (3.18) for the mean field is valid only in the vicinit of the maximum.

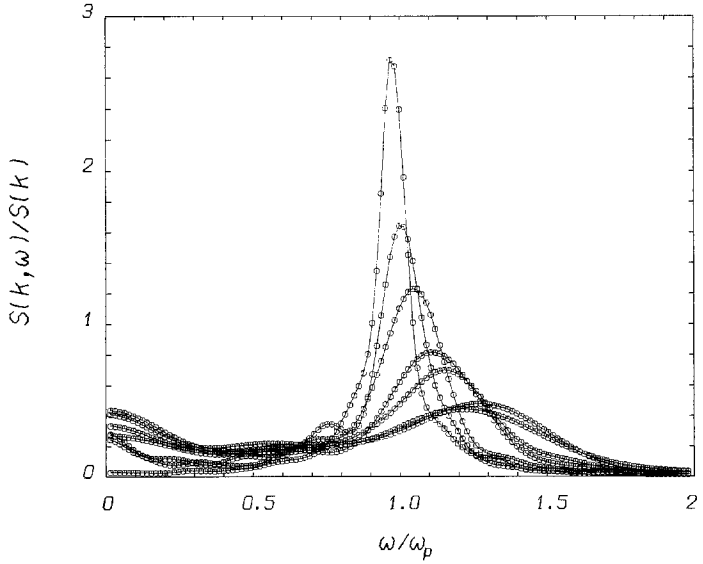

Fig. 8. MD-generated dynamic structure factor $S(k, \omega)/S(k)$ versus ω/ω_p for $\sigma/a = 0.177$, $\Gamma = 1$, and, from left to right, peak positions for $q = ak = 0$; 0.275; 0.389; 0.550; 0.615; 0.778; and 0.825.

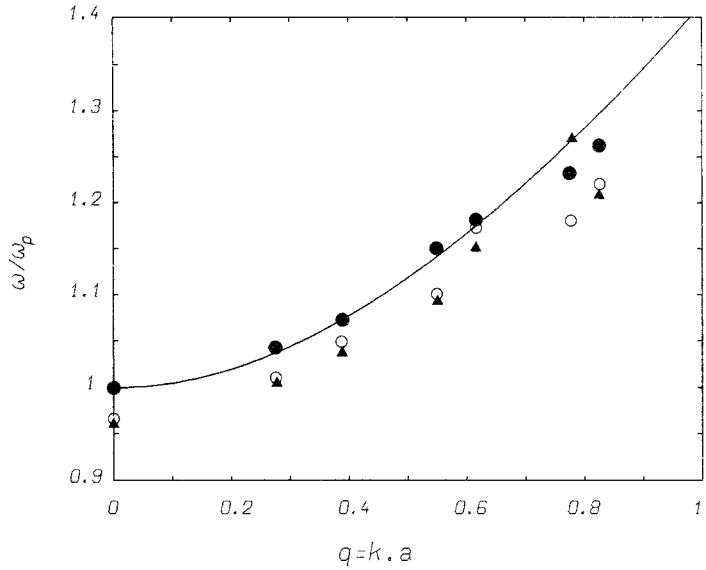

Fig. 9. Dispersion curves $\omega(k)$ for the plasmon resonance frequency as a function of $q = ak$, as determined from the peak positions of the MD-generated $S(k, \omega)$ at $\Gamma = 1$; (●) $\sigma/a = 1$; (○) $\sigma/a = 0.35$; (▲) $\sigma/a = 0.177$. (–) The classic Vlasov result for the homogeneous OCP.

plasmon resonance is shifted above ω_p.[13] This difference may be ascribed to the binding nature of the 2D Coulomb potential at large distances, which does not carry over to 3D.

We made no attempt to extend the mean field calculations to finite wavenumbers because of the considerable technical difficulties involved. Typical MD results for $S(k, \omega)$ at several wavenumbers k are shown[5] in Fig. 8, and the corresponding dispersion curves for three densities are compared in Fig. 9 to the classic Vlasov result for the electron plasma in a uniform background (i.e., the OCP). The periodic field of the ions is seen

[5] These results can be used for estimating $s(\omega)$ by extrapolation methods. The spectra $S(k, \omega)/S(k)$ (for small k) are represented by Lorentzians with a good accuracy. Therefore, their peaks have heights that are inversely proportional to the damping. The measured values of the damping at finite k are well fitted by the expression $\gamma_0 + \delta_L(k)$, where γ_0 is the residual damping at $k = 0$ and $\delta_L(k)$ is the Landau damping. The fit value of γ_0 leads to a peak of $s(\omega)$ that is 30% smaller than the result obtained from $\mathbf{J}(t)$. This disagreement might be due to the considerable statistical noise in $\mathbf{J}(t)$, and also to finite resolution effects arising from the tightness of the peak. This suggests that our indirect calculation of $s(\omega)$ leads to a relatively large uncertainty in the height of the peaks. The corresponding uncertainty relating to the wings of the spectrum is surely much smaller, as illustrated by the good second and fourth moments determined from MD data. Note that the mean field prediction regarding $s(\omega_m)$ is in reasonable agreement with the MD extrapolated value.

to have little influence on the dispersion curve at intermediate couplings ($\Gamma \simeq 1$), except for a general downward shift at the lower densities. In particular, the present model does not lead to the oscillatory dispersion observed with the hard-core model,[3] which may be ascribed to the stronger perturbation of the electron trajectories induced by the ionic lattice in that case.

5. DISCUSSION

In this series of papers we have presented the first systematic investigation of a Vlasov-like kinetic equation for a plasma in a periodic field. The solution of the equation presents considerable technical difficulties, but a number of general results can be obtained, including the absence of a dielectric plasma transition or the form of the static structure factor. As is generally the case for a mean field theory, general (qualitative) results are independent of dimensionality, but explicit calculations of specific properties, such as the long-wavelength charge fluctuation spectrum, are relatively easy in 1D only. In the present paper we have confronted the mean field predictions with MD simulation results in 2D. This comparison is limited by the fact that MD simulations cannot in practice be extended below $\Gamma \simeq 1$, while the complexity of the mean field theory allows only the explicit calculation of the dominant high-temperature deviations from the uniform background limit, which are $O(\Gamma^3)$ for the structure factor and the screening length and $O(\Gamma^{3/2})$ for the charge fluctuation spectrum $s(\omega)$. This means that the validity of the mean field results is *a priori* limited to $\Gamma < 1$. Moreover, since the perturbation due to the periodic field of the ions is strongest at low density, the high-temperature limitation is *a priori* more severe in that regime. Taking into account the above restrictions and the uncertainties specific to the MD indirect calculation of $s(\omega)$, the quantitative predictions of the mean field theory for a coupling as strong as $\Gamma \simeq 1$ turn out to be reasonable. The latter faithfully reproduces the general trends observed in the MD results for the shift and damping of the plasmon mode. The excessive damping predicted by mean field theory at low densities is probably a direct consequence of the additional limitation to the dominant high-temperature contribution. When σ/a approaches 1, the mean field predictions become more accurate. However, the mean field damping is less than that observed in the MD results, as one would expect, since electron–electron collisions lead to an additional damping mechanism not included in the kinetic theory. We believe that, in view of the encouraging agreement observed for $\Gamma \simeq 1$, mean field theory should be very reliable at higher temperatures.

APPENDIX

In this appendix we derive the high-temperature expressions (3.15a) and (3.15b) for $R(\omega)$ and $I(\omega)$. For this purpose, we first study the high-energy trajectories of one electron in the auxiliary potential $V_{L,s}(\mathbf{r})$ defined by Eq. (3.13). This allows us to compute the dominant contributions to $W_1(\omega)$ and $W_2(\omega)$ in the high-temperature limit. The resulting high-temperature expansions of $R(\omega)$ and $I(\omega)$ are then obtained. Furthermore, the expressions (3.16) of the functions $r(\omega)$ and $i(\omega)$, which are involved in these expansions, are reduced in favor of more explicit and simpler formulas. For notational convenience, we set $\mathbf{r}(t) \equiv \mathbf{r}_{cl}(t; \mathbf{r}, \mathbf{v})$ and $\mathbf{v}(t) \equiv \mathbf{v}_{cl}(t; \mathbf{r}, \mathbf{v})$.

The high-energy trajectories with an initial velocity $\mathbf{v}$ nonorthogonal to any of the $\mathbf{G}_j$ have been studied in the text. The cases where $\mathbf{v}$ is "almost" orthogonal to $\mathbf{G}_i$ $(1 \leqslant i \leqslant s)$ can be treated as follows. Let (x, y) be the orthonormal Cartesian frame where the unit vector in the x direction is $\hat{\mathbf{G}}_i$. We want to investigate the behavior of $\mathbf{u}(t) = \mathbf{v}(t) - \mathbf{v}$ when $|v_y| \to \infty$, v_x kept fixed. Integrating the equations of motion, we obtain

$$\mathbf{u}(t) = -\frac{1}{m} \int_0^t dt' \frac{\partial V_{L,s}}{\partial \mathbf{r}} (\mathbf{r}(t')) \tag{A1}$$

Since the force $-\partial V_{L,s}/\partial \mathbf{r}$ is bounded, we infer from (A1)

$$|\mathbf{u}(t)| \leqslant \frac{t}{m} \operatorname*{Sup}_{\mathbf{r} \in \mathrm{WS}} \left(\left| \frac{\partial V_{L,s}}{\partial \mathbf{r}} \right| \right) \tag{A2}$$

The upper bound (A2) does not depend on the initial velocity, so $|\mathbf{u}(t)|$ as well as $u_x(t)$ and $u_y(t)$ remain bounded (at fixed times) when $|v_y| \to \infty$. Furthermore, the conservation of the energy gives

$$v_y u_y(t) = \frac{1}{m} [V_{L,s}(\mathbf{r}) - V_{L,s}(\mathbf{r}(t))] - \frac{1}{2} u^2(t) - v_x u_x(t) \tag{A3}$$

from which we obtain by using (A2)

$$|v_y u_y(t)| \leqslant \frac{2}{m} \operatorname*{Sup}_{\mathbf{r} \in \mathrm{WS}} [|V_{L,s}(\mathbf{r})|] + \frac{t^2}{2m^2} \left[\operatorname*{Sup}_{\mathbf{r} \in \mathrm{WS}} \left(\left| \frac{\partial V_{L,s}}{\partial \mathbf{r}} \right| \right) \right]^2 + |v_x| \frac{t}{m} \operatorname*{Sup}_{\mathbf{r} \in \mathrm{WS}} \left(\left| \frac{\partial V_{L,s}}{\partial \mathbf{r}} \right| \right) \tag{A4}$$

Since the upper bound (A4) does not depend on v_y, $|u_y(t)|$ remains bounded by const/$|v_y|$ when $|v_y| \to \infty$. This implies

$$v_y(t) = v_y + O(1/v_y), \qquad y(t) = y + v_y t + O(1/v_y) \tag{A5}$$

when $|v_y| \to \infty$. Taking into account (A5), the equation of motion along the x axis becomes

$$m\frac{d^2x}{dt^2}(t) = 2\sum_{p=1}^{\infty} pG_i \hat{V}_L(p\mathbf{G}_i)\sin[pG_i x(t)] + 2\sum_{\substack{j=1 \\ j\neq i}}^{s}\sum_{p=1}^{\infty} pG_{jx}\hat{V}_L(p\mathbf{G}_j) \times \sin(pG_{jx}x(t) + pG_{jy}y + pG_{jy}v_y t) + O\left(\frac{1}{v_y}\right) \tag{A6}$$

Neglecting terms $O(1/v_y)$, we then see that the calculation of $x(t)$ is reduced to a purely one-dimensional problem, where a particle is submitted to the force deriving from the potential

$$U_i(x) = 2\sum_{p=1}^{\infty} \hat{V}_L(p\mathbf{G}_i)\cos(pG_i x) \tag{A7}$$

and to time-dependent forces oscillating rapidly in time with frequencies proportional to v_y. The corresponding motion can be studied by a perturbative treatment of the time-dependent forces[14]: the first corrections to the unperturbed motion in the potential $U_i(x)$ are $O(1/v_y)$ for the velocity and $O(1/v_y^2)$ for the position. Thus, we finally have

$$v_x(t) = v_i(t) + O(1/v_y), \qquad x(t) = x_i(t) + O(1/v_y) \tag{A8}$$

where $(x_i(t), v_i(t))$ are the position and the velocity of a particle moving in $U_i(x)$ with the initial conditions $x_i(0) = x_i = \mathbf{r}\cdot\hat{\mathbf{G}}_i$ and $v_i(0) = v_i = \mathbf{v}\cdot\hat{\mathbf{G}}_i$. Both Eqs. (A5) and (A8) represent the laws of motion in the limit $|v_y| \to \infty$ (t and v_x being kept fixed).

Now we turn to the high-temperature forms of $W_1(\omega)$ and $W_2(\omega)$. We first consider the case of $W_1(\omega)$. Before taking the high-temperature limit, it is convenient to transform the expression (I.6.7) of $W_1(\omega)$ in the following way. Performing an integration by parts in $\int_0^\infty dt...$, we find $[\varphi(v) = (\beta m/2\pi)\exp(-\beta m v^2/2)]$

$$W_1(\omega) = \frac{1}{2}\chi_D^2 \int_{WS\otimes\mathbb{R}^2} d\mathbf{r}\, d\mathbf{v}\, \rho(\mathbf{r})\,\varphi(v) \times \left\{\lim_{\eta\to 0^+}\int_0^\infty dt \exp(i\omega t - \eta t)\,[\mathbf{r}(t) - \mathbf{r}]\cdot\mathbf{v}(t)\right\} \tag{A9}$$

which becomes, after introducing $\mathbf{u}(t)$,

$$W_1(\omega) = -\frac{\omega_p^2}{\omega^2} + \frac{\chi_D^2}{2} \int_{WS \otimes \mathbb{R}^2} d\mathbf{r}\, d\mathbf{v}\, \rho(\mathbf{r})\, \varphi(v) \left\{ \lim_{\eta \to 0^+} \int_0^\infty dt \exp(i\omega t - \eta t) \right.$$
$$\left. \times \left[t\mathbf{v} \cdot \mathbf{u}(t) + \int_0^t dt'\, \mathbf{v} \cdot \mathbf{u}(t') + \int_0^t dt'\, \mathbf{u}(t) \cdot \mathbf{u}(t') \right] \right\} \tag{A10}$$

Furthermore, the conservation of the energy can be written as

$$\mathbf{v} \cdot \mathbf{u}(t) = \frac{1}{m} [V(\mathbf{r}) - V(\mathbf{r}(t))] - \frac{1}{2} u^2(t) \tag{A11}$$

Multiplying both sides of (A11) by $\rho(\mathbf{r})\, \varphi(v)$ and taking the average over $WS \otimes \mathbb{R}^2$, we obtain

$$\int_{WS \otimes \mathbb{R}^2} d\mathbf{r}\, d\mathbf{v}\, \rho(\mathbf{r})\, \varphi(v) \mathbf{v} \cdot \mathbf{u}(t) = -\frac{1}{2} \int_{WS \otimes \mathbb{R}^2} d\mathbf{r}\, d\mathbf{v}\, \rho(\mathbf{r})\, \varphi(v)\, u^2(t) \tag{A12}$$

where we have also used Lemma L1 of paper I, which implies that

$$\int_{WS \otimes \mathbb{R}^2} d\mathbf{r}\, d\mathbf{v}\, \rho(\mathbf{r})\, \varphi(v) [V(\mathbf{r}) - V(\mathbf{r}(t))] = 0$$

Using (A12) in (A10), we rewrite $W_1(\omega)$ as

$$W_1(\omega) = -\frac{\omega_p^2}{\omega^2} + \frac{\chi_D^2}{2} \int_{WS \otimes \mathbb{R}^2} d\mathbf{r}\, d\mathbf{v}\, \rho(\mathbf{r})\, \varphi(v) \left\{ \lim_{\eta \to 0^+} \int_0^\infty dt \exp(i\omega t - \eta t) \right.$$
$$\left. \times \left[\int_0^t dt'\, \mathbf{u}(t') \cdot \mathbf{u}(t) + \frac{1}{2i\omega} (1 - i\omega t)\, u^2(t) \right] \right\} \tag{A13}$$

In the high-temperature regime, the dominant contributions to $W_1(\omega)$ arise from the high-energy trajectories in the ionic potential $V_L(\mathbf{r})$. For technical reasons, it is convenient to first compute these contributions with the auxiliary potential $V_{L,s}(\mathbf{r})$ in place of $V_L(\mathbf{r})$ and to take the limit $x \to \infty$ at the end. For the high-energy trajectories with an initial velocity non-orthogonal to any of the $\mathbf{G}_j$ $(1 \leqslant j \leqslant s)$, we find from (3.14)

$$\lim_{\eta \to 0^+} \int_0^\infty dt \exp(i\omega t - \eta t) \left[\int_0^t dt'\, \mathbf{u}(t') \cdot \mathbf{u}(t) + \frac{1}{2i\omega} (1 - i\omega t)\, u^2(t) \right]$$
$$= O\left(\frac{1}{v^2}\right) \tag{A14}$$

while for the high-energy trajectories with an initial velocity "almost" orthogonal to $\mathbf{G}_i$, we find from (A5) and (A8)

$$\lim_{\eta \to 0^+} \int_0^\infty dt \cdots = \lim_{\eta \to 0^+} \int_0^\infty dt \exp(i\omega t - \eta t) \left\{ (x_i(t) - v_i t - x_i)[v_i(t) - v_i] + \frac{1}{2i\omega}(1 - i\omega t)[v_i(t) - v_i]^2 \right\} + O\left(\frac{1}{v}\right) \tag{A15}$$

Thus, if we look at the variations of $\lim_{\eta \to 0^+} \int_0^\infty dt \cdots$ with respect to the polar angle θ of $\mathbf{v}$, for v fixed high enough, we see that this quantity has $2s$ peaks located at $\{\theta_j, \theta_j + \pi, 1 \leqslant j \leqslant s\}$, where $\theta_j - \pi/2$ is the polar angle of $\mathbf{G}_j$. Since these peaks have heights and widths that are $O(1)$ and $O(1/v)$, respectively, their contributions to the angular integral $\int_0^{2\pi} d\theta \{\lim_{\eta \to 0^+} \int_0^\infty dt \cdots\}$ are $O(1/v)$. The corresponding contributions of the other regions are $O(1/v^2)$ and can then be neglected. Therefore, we obtain, after making the variable change $\theta = \theta_j + v_j/v$ in the vicinity of each peak,

$$\begin{aligned} &\int_0^{2\pi} d\theta \left\{ \lim_{\eta \to 0^+} \int_0^\infty dt \cdots \right\} \\ &\quad = \frac{2}{v} \sum_{j=1}^{s} \int_{-\infty}^{\infty} dv_j \left(\lim_{\eta \to 0^+} \int_0^\infty dt \exp(i\omega t - \eta t) \right. \\ &\qquad \times \left\{ [x_j(t) - v_j t - x_j)(v_j(t) - v_j] \right. \\ &\qquad \left. \left. + \frac{1}{2i\omega}(1 - i\omega t)[v_j(t) - v_j]^2 \right\} \right) + O\left(\frac{1}{v^2}\right) \end{aligned} \tag{A16}$$

Using (A16) in (A13) and taking the limit $s \to \infty$, we finally obtain

$$\begin{aligned} W_1(\omega) = &-\frac{\omega_p^2}{\omega^2} + \frac{\Gamma^{3/2}}{\pi^{1/2} a^3 \omega_p} \\ &\times \sum_{j=1}^{\infty} \int_{\mathrm{WS}} d\mathbf{r} \int_{-\infty}^{\infty} dv_j \left(\lim_{\eta \to 0^+} \int_0^\infty dt \exp(i\omega t - \eta t) \right. \\ &\times \left\{ [x_j(t) - v_j t - x_j][v_j(t) - v_j] \right. \\ &\left. \left. + \frac{1}{2i\omega}(1 - i\omega t)[v_j(t) - v_j]^2 \right\} \right) + o(\Gamma^{3/2}) \end{aligned} \tag{A17}$$

(in order to test the validity of the present calculation, we have checked that the integral $\int_{-\infty}^{\infty} dv_j \cdots$ as well as the series $\sum_{j=1}^{\infty} \cdots$ do converge). A similar analysis of $W_2(\omega)$ shows that $W_2(\omega)$ is $O(\Gamma^2)$. Therefore, up to the order $\Gamma^{3/2}$ included, $R(\omega)$ and $I(\omega)$ are entirely determined by $W_1(\omega)$. Replacing $W_1(\omega)$ by (A17) in (3.12b), (3.12c), we then find the high-temperature expansions (3.15a), (3.15b) of $R(\omega)$ and $I(\omega)$.

The expression (3.16) of $r_j(\omega)$, as well as the corresponding expression of $i_j(\omega)$, can be simplified as follows. Since $\int_{-\infty}^{\infty} dv_j \cdots$ only depends on x_j, the integration upon y_j in $\int_{\mathrm{WS}} d\mathbf{r} \cdots$ can be easily performed. The remaining integral upon x_j involves the product of $\int_{-\infty}^{\infty} dv_j \cdots$ by a function of x_j which is the reunion of straight segments. Using the symmetry and periodicity properties of $\int_{-\infty}^{\infty} dv_j \cdots$, we then find

$$\int_{\mathrm{WS}} d\mathbf{r} \int_{-\infty}^{\infty} dv_j \left\{ \lim_{\eta \to 0^+} \int_0^{\infty} dt \cdots \right\}$$

$$= 4bN_j^{1/2} \int_0^{\lambda_j} dx_j \int_{-\infty}^{\infty} dv_j \left\{ \lim_{\eta \to 0^+} \int_0^{\infty} dt \cdots \right\} \tag{A18}$$

with $N_j = m_j^2 + n_j^2 - m_j n_j$ and $\lambda_j = \pi/G_j = b\sqrt{3}/(2\sqrt{N_j})$ [$2\lambda_j$ is the spatial period of the potential $U_j(x)$]. Furthermore, the quantity

$$\int_0^{\lambda_j} dx_j \int_{-\infty}^{\infty} dv_j \left\{ \lim_{\eta \to 0^+} \int_0^{\infty} dt \cdots \right\}$$

can be transformed using the same methods as those applied to the reduction of similar quantities in paper II. The final results are ($\mathcal{P}\mathcal{P}$ is the principal part)

$$r_j(\omega) = -\frac{8bN_j^{1/2}}{\pi^{3/2} m\omega_p a^5 \omega} \mathcal{P}\mathcal{P}$$

$$\times \int_{U_j(0)}^{\infty} dE \left\{ P(\omega T(E)) \left[\int_0^{T(E)} dt \cos(\omega t)\, v_0(t) \right]^2 \right.$$

$$+ \int_0^{T(E)} dt \sin(\omega t)\, v_0(t) \int_0^{T(E)} dt \cos(\omega t)\, v_0(t)$$

$$+ \int_0^{T(E)} dt' \int_{t'}^{T(E)} dt \sin(\omega t - \omega t')\, v_0(t)\, v_0(t')$$

$$\left. - \frac{1}{\omega} \int_0^{T(E)} dt\, v_0^2(t) \right\} \tag{A19}$$

and

$$i_j(\omega) = \frac{8bN_j^{1/2}}{\pi^{1/2} m\omega_p a^5 \omega^2} \left\{ \sum_{n=0}^{\infty} \frac{[\int_0^{(n+1/2)\pi/\omega} dt\, v_0(t)\cos(\omega t)]^2}{(dT/dE)(E_{n,<})} - \sum_{n=1}^{\infty} \frac{[\int_0^{n\pi/\omega} dt\, v_0(t)\cos(\omega t)]^2}{(dT/dE)(E_{n,>})} \right\} \tag{A20}$$

with

$$T(E) = \begin{cases} \displaystyle\int_0^{x_m(E)} dx \left\{ \frac{2}{m}[E - U_j(x)] \right\}^{-1/2}, & E < U(\lambda_j) \\ \displaystyle\int_0^{\lambda_j} dx \left\{ \frac{2}{m}[E - U_j(x)] \right\}^{-1/2}, & U(\lambda_j) < E \end{cases} \tag{A21}$$

and

$$P(\omega T(E)) = \begin{cases} -\mathrm{tg}[\omega T(E)], & E < U(\lambda_j) \\ \mathrm{cotg}[\omega T(E)], & U(\lambda_j) < E \end{cases} \tag{A22}$$

The resonant energies $E_{n,<}$ and $E_{n,>}$ are such that $T(E_{n,<}) = (n+1/2)\pi/\omega$ and $T(E_{n,>}) = n\pi/\omega$; $v_0(t)$ is the velocity corresponding to the initial conditions $x_0(0) = 0$ and $v_0(0) = \{2[E - U_j(0)]/m\}^{1/2}$, and $x_m(E)$ is the turning point corresponding to the energy E, i.e., $U(x_m(E)) = E$. For deriving the above expressions, we have assumed that $U_j(x)$ monotonically increases from $U_j(0)$ to $U_j(\lambda_j)$ [the conditions $E < U(\lambda_j)$ or $U(\lambda_j) < E$ then correspond to confined or unconfined motions]. If this hypothesis is not satisfied, the previous expressions have to be slightly modified.

Finally, let us conclude this Appendix by some comments regarding the expressions (A19), (A20). First, the latter are well defined, i.e., the integral $\int_{U_j(0)}^{\infty} dE \ldots$ and the series $\sum_{n=0}^{\infty} \ldots$ and $\sum_{n=1}^{\infty} \ldots$ do converge. Indeed, the integrant of $\int_{U_j(0)}^{\infty} dE \ldots$ decays like $1/E^{3/2}$ when $E \to \infty$, while the generic terms of the previous series decay exponentially[7] when $n \to \infty$. Although the potential $U_j(x)$ defined by Fourier series (A7) can be expressed in terms of elementary functions, the various quadratures involved in (A19), (A20) cannot be analytically computed, except when $\sigma = 0$. In the latter case, $U_j(x)$ reduces to the reunion of arcs of parabolas, and (A19) and (A20) become proportional to the explicit expressions (II.4.45) and (II.4.46) given in paper II. For $\sigma \neq 0$, the resonant energies $E_{n,<}$ and $E_{n,>}$, as well as the other ingredients of (A20), are determined numerically; since the series $\sum_{n=0}^{\infty} \ldots$ and $\sum_{n=1}^{\infty} \ldots$ converge exponentially fast, $i_j(\omega_p)$ is then calculated with a good accuracy be keeping only a few terms in these series. The numerical calculation of $r_j(\omega_p)$ is more cumbersome, and not really essential, for the reasons given in the text. The quantities $i_j(\omega_p)$ are found to decay rapidly when j increases [this is due to the

fact that $U_j(x)$ then becomes more and more flat and small]. For the values of σ considered in the text, $i(\omega_p) = \sum_{j=1}^{\infty} i_j(\omega_p)$ is practically determined by the first three groups of terms:

$$j = \begin{cases} 1, & \mathbf{G}_1 = \mathbf{A} \\ 2, & \mathbf{G}_2 = \mathbf{B} \\ 3, & \mathbf{G}_3 = \mathbf{A} + \mathbf{B} \end{cases} \qquad (N_1 = N_2 = N_3 = 1)$$

$$j = \begin{cases} 4, & \mathbf{G}_4 = \mathbf{A} - \mathbf{B} \\ 5, & \mathbf{G}_5 = 2\mathbf{A} + \mathbf{B} \\ 6, & \mathbf{G}_6 = \mathbf{A} + 2\mathbf{B} \end{cases} \qquad (N_4 = N_5 = N_6 = 3)$$

$$j = \begin{cases} 7, & \mathbf{G}_7 = 2\mathbf{A} - \mathbf{B} \\ 8, & \mathbf{G}_8 = \mathbf{A} - 2\mathbf{B} \\ 9, & \mathbf{G}_9 = 3\mathbf{A} + \mathbf{B} \\ 10, & \mathbf{G}_{10} = \mathbf{A} + 3\mathbf{B} \\ 11, & \mathbf{G}_{11} = 3\mathbf{A} + 2\mathbf{B} \\ 12, & \mathbf{G}_{12} = 2\mathbf{A} + 3\mathbf{B} \end{cases} \qquad (N_7 = \cdots = N_{12} = 7)$$

For $\sigma = 0$, i.e., for point ions, the series $\sum_{j=1}^{\infty} i_j(\omega)$ and $\sum_{j=1}^{\infty} r_j(\omega)$ diverge. In this case, the present perturbative analysis of the contributions of the high-energy trajectories is not applicable, because however high its energy, one electron may be scattered in arbitrary directions by one ion if the impact distance of the electron–ion collision is small enough. The functions $(R(\omega) + \omega_p^2/\omega^2)$ and $I(\omega)$ should then go to zero slower than $\Gamma^{3/2}$ in the high-temperature limit.

REFERENCES

1. J. M. Kosterlitz and D. J. Thouless, *J. Phys. C* **6**:1181 (1973).
2. J. Fröhlich and T. Spencer, *Phys. Rev. Lett.* **46**:1006 (1981).
3. J. Clérouin and J. P. Hansen, *Phys. Rev. Lett.* **54**:2277 (1985); J. Clérouin, J. P. Hansen, and B. Piller, *Phys. Rev. A* **36**:2793 (1987).
4. J. Clérouin, J. P. Hansen, and B. Piller, *Europhys. Lett.* **4**:771 (1987).
5. A. Alastuey and J. P. Hansen, *Europhys. Lett.* **2**:97 (1986).
6. A. Alastuey, *J. Stat. Phys.* **48**:839 (1987).
7. A. Alastuey, *J. Stat. Phys.* **49**:685 (1987).
8. A. Lenard, *J. Math. Phys.* **2**:682 (1961).
9. E. H. Hauge and P. C. Hemmer, *Phys. Norv.* **5**:209 (1971).
10. P. Vieillefosse and J. P. Hansen, *Phys. Rev. A* **12**:1106 (1975).
11. L. Verlet, *Phys. Rev.* **159**:98 (1967).
12. J. P. Hansen, I. R. McDonald, and E. L. Pollock, *Phys. Rev. A* **11**:1025 (1975).
13. J. P. Hansen and I. R. McDonald, *Phys. Rev. A* **23**:2041 (1982).
14. L. Landau and E. Lifschitz, *Physique Théorique*, Vol. I, *Mécanique* (Mir, Moscow, 1969).